INVESTIGATING MEDIUM AND HEAVY MASS HEAVY-ION FUSION REACTIONS AND BARRIER DISTRIBUTIONS WITH COUPLED-CHANNEL ANALYZES

B. Erol

Department of Physics, Recep Tayyip Erdogan University, 53100 Rize, Turkey

Z.M. Cinan, T. Baskan, A.H. Yilmaz

Department of Physics, Karadeniz Technical University, 61080 Trabzon, Turkey

(Received February 18, 2021; accepted July 10, 2021)

The fusion process is the effect of a one-dimensional barrier penetration model that incorporates scattering potential as a combination of Coulomb and proximity potentials. Heavy-ion fusion reactions were performed with coupled-channel (CC) calculations. In heavy-ion fusion reactions, CC formalism is carried through the under-barrier energy. Here, fusion cross sections were calculated and investigated for the O^{16}+$Ge^{70,72,74,76}$, O^{16}+$Sm^{148,150,152,154}$, Ne^{20}+$Zr^{90,92,94,96}$, Ne^{20}+$Sn^{112,114,116,118,120}$, Si^{28}+$Mo^{90,96}$, Si^{28}+$Mg^{24,26}$, Si^{28}+$Ni^{58,64}$, Si^{28}+$Zr^{90,94,96}$, S^{32}+$Zr^{90,96}$, S^{36}+$Pb^{204,206,208,210}$, Ar^{40}+$Hf^{176,178,180}$ in the framework of CC calculations (CCFULL, NRV) and Wong's formula. Fusion cross sections were analyzed in detail by CC calculations considering 2^+ and 3^- excitation modes for the projectile and the target. The calculated cross-section results were compared with the experimental data. The calculations were found to produce reliable data compared to experimental data. Fusion barrier distributions ($D_{\rm fus}$) for all reactions have been investigated below and above the Coulomb barrier using the coupled-channel method with CCFULL, NRV codes and second derivative of Wong's formula. The harmony among these calculations was examined and it was determined that the models were in harmony with each other.

DOI:10.5506/APhysPolB.52.1117

1. Introduction

Heavy-ion collisions have been of interest for experimenters and theorists for the last few decades. The existence of open reaction channels is used to identify the collisions. The paper is devoted to the theoretical study

of the dynamics of heavy-ion fusion by using the processes of elastic scattering, inelastic scattering and mainly the fusion reactions around the Coulomb barrier [1]. Analyzing heavy-ion fusion cross sections of the Coulomb barrier is a combination of nuclear interaction: the repulsive long-range Coulomb centrifugal potentials and attractive, short-range nuclear potential. The total potential reaches a maximum at which the nuclei are captured and fused when the repulsive Coulomb force and the attractive nuclear forces balance each other and the relative motion energy exceeds this potential [2]. Depending on the bombarding energy, a number of masses of the target and the projectiles different perceptions occur in heavy-ion collisions. In this paper, the energy range is near and below the Coulomb barrier for the fusion reaction . The fusion cross section in heavy-ion collisions at energies slightly above the Coulomb barrier can be clearly explained by a simple potential model that only depends on the relative distance between the reacting nuclei. It was shown by the theoretical works that the increase of the fusion cross section was due to the mapping of the relative movement among the collision and other degrees of freedom of the nucleus. These are called channel-coupling effects [1, 3, 4]. It is now well-understood that the experimental data of fusion reaction at sub-barrier energies, *i.e.* fusion cross section and fusion barrier distribution, can be well-explained by the coupled-channel formalism. This formalism takes into account the coupling between the relative motion and the intrinsic degrees of freedom such as nuclear vibration, rotational excitation as well as the transfer processes of the colliding nuclei [5–7]. For investigating the effects of channel coupling in more details, the concept of fusion barrier distribution which is defined as the second derivative of the product of the center-of-mass energy, E, and the fusion cross section with respect to E, *i.e.* $D_{\mathrm{fus}} = \mathrm{d}^2[Es]\mathrm{d}E^2$ is proposed [8–11]. It has also been shown that this concept can be used as a powerful tool to study the channel coupling effects on heavy-ion fusion reactions at sub-barrier energies [7, 12, 13]. We investigated the fusion cross sections of the O^{16}+$Ge^{70,72,74,76}$ reaction system with CCFULL [2], NRV [14] coupled-channel codes and Wong's formalism in the 30–55 MeV-cm energy range. These four systems were examined in the literature by Aguilera *et al.* [15], both experimentally and with CCDEF [16] coupled-channel calculation code. The fusion cross sections of O^{16}+$Sm^{148,150,152,154}$ are compared with experimental data [17] and CCFULL code of CC calculation [1]. We examined the fusion cross-section reactions of the Ne^{20}+$Zr^{90,92,94,96}$ and Ne^{20}+$Sn^{112,114,116,118,120}$ reaction systems with CCFULL, NRV coupled-channel codes and Wong's formalism in the 40–80 MeV-cm energy range. Si^{28}+$Mg^{24,26}$ reaction system was carried out in experimental work by Morsad *et al.* [18], as well as using a modified version of the simplified coupled-channel code CCFUS. Si^{28}+$Ni^{58,64}$ reaction set was studied experimentally by Stefanini *et al.* [19]. Si^{28}+$Zr^{90,94}$ reaction

set was experimentally studied by Kalkal *et al.* [20] and their experimental data were presented in the literature. In the same study, they made calculations with CCFULL code. Experimental and coupled-channel methods of Si^{28}+$Mo^{90,96}$ reaction group were used by Ackermann *et al.* [21]. S^{32}+$Zr^{90,96}$ reactions were studied in the 65–100 MeV-cm energy range by Zhang *et al.* [22] both with CCDEF coupled-channel code and experimentally. S^{36}+$Pb^{204,206,208,210}$ reactions were studied using CCFULL, NRV coupled-channel codes and Wong's formalism, and fusion cross-section results were compared with the study conducted in 2012 by Khuyagbaatur *et al.* [23], where CCFULL and experimental data were given together. For the reaction system of Ar^{40}+$Hf^{176,178,180}$, the cross-section results are compared with experimental data [24]. The aim of this paper is to work on the code or codes and numerical calculation methods that make fusion cross-section calculations and to determine the methods that give the most accurate and closest results according to the experimental results, and this way to provide clear information about the reactions and also for the reaction groups without experimental data, comparing the calculation methods included in the study and to show how the small or big similarities and differences between the methods affect the results. The importance of the fusion barrier distribution has made the subject an interesting focus for many researchers [25–27]. There are two main features used to understand and define the fusion barrier, the barrier position (R_b) and the barrier height (V_b) [28]. The shape of the barrier distribution gives important information about reaction dynamics and colliding core structures [29, 30]. To obtain an accurate fusion barrier distribution, high-quality fusion cross-section data are required, as well as a good numerical method to calculate the second derivative. For this purpose, we compared the fusion barrier distributions obtained by theoretical calculations using CCFULL code and NRV code with the second derivative of Wong's formula [25]. Fusion barrier distributions (D_{fus}) have been investigated below and above the Coulomb barrier using coupled-channel method with CCFULL, NRV codes and second derivative of Wong's formula under coupling values.

2. Methodology

2.1. Coupled-channel formalism

To explain the possibility of exciting collective degrees of freedom of the target and/or projectile on their way to fusion, we used the finite range version of the simplified coupled-channel program, CCFULL [2]. The CCFULL analyzes the CC equations to calculate the fusion cross sections. It takes into account the couplings for all orders. You must take $Z_P + Z_T > 12$ and the charge product $Z_P Z_T < 1800$. For this code, CC equations can be

read [2, 31]

$$\left[-\frac{\hbar^2}{2\mu}\frac{\mathrm{d}^2}{\mathrm{d}r^2}+\frac{J(J+1)\hbar^2}{2\mu r^2}+V_N^0(r)+\frac{Z_\mathrm{P}Z_\mathrm{T}e^2}{r}+\varepsilon_n-E\right]\psi_n(r)+\sum_m V_{nm}(r)\psi_m(r)=0\,. \tag{1}$$

μ is the reduced mass, r is the relative motion of radial component's coordinate, e is the elementary charge, ε_n is the excitation energy for each channel, E is the center-of-mass energy, V_{nm} are the matrix elements of the coupling Hamiltonian, Z_P and Z_T are the charge numbers of the projectile and the target, and V_N^0 is the nuclear potential Woods–Saxon parametrization in the program [32]

$$V_\mathrm{N}^0(r)=\frac{-V_0}{1+\exp\left[\left(r-R_0\right)/a_0\right]} \tag{2}$$

with $R_0=r_0\left(A_\mathrm{P}^{1/3}+A_\mathrm{T}^{1/3}\right)$.

There is no limit to the CC and this makes the calculation of heavy nuclei useful for the synthesis of super-heavy elements. In collisions of heavy nuclei, the cross section of compound nucleus formation is

$$\sigma_\mathrm{fus}^\mathrm{CN}=\frac{\pi\hbar^2}{2\mu E}\sum_{l=0}^{\infty}(2l+1)T_l(E)P_\mathrm{CN}(E,l)\,. \tag{3}$$

Here, P_CN is the probability of compound nucleus formation by two nuclei coming in contact, $T_l(E)$ is the transmission coefficient [2].

NRV is a new algebraic method used for the numerical solution of the Schrödinger equation group combined in fusion reactions [33, 34]. According to the user's requirement, it provides also the possibility to work with the proximity potential and takes into account the so-called geometric factor in the potential that is quite important when large deformations play a role, and provide a convenient interface [14]. Although NRV and CCFULL seem the same in terms of input and output, the biggest feature that distinguishes them from each other is the matrix element calculation forms [2, 33].

2.2. Fusion barrier distribution

Coupling with intrinsic degrees of freedom causes the effect of changing the height of the barrier and dispersing the barrier into fusion. Barrier distributions (BDs) are highly sensitive to high-grade nuclear deformations. In other words, BDs can be used as a powerful tool to learn about the structure of the interacting nuclei. BDs can be determined by precise measurements of the fusion excitation function. It has consequences for the channel caused by

the distribution of fusion barriers. Here, the experimental barrier is closely related to the coupled-channel (CC) fusion model [12, 35]. In 1991, it was shown that there is a real distribution of probabilities of finding a fusion barrier in E_{cm} in a given center-of-mass energy. In the same year, it was shown that the actual distribution of probabilities of finding a fusion barrier in a given center-of-mass energy can be derived directly from the exact experimental fusion sections with σ. According to Rowley *et al.* [11], Siwek-Wilczyńska and Wilczyński [36], fusion barrier distributions can be gotten from the experimental data as in Eq. (4) [37]

$$D_{\mathrm{fus}}(E) = \frac{\mathrm{d}^2(E\sigma)}{\mathrm{d}E^2}\,. \tag{4}$$

Wong's formula

Wong's formula for the barrier distribution is derived as an alternative to the three-point difference formula, which requires a large number of experimental points. This is a method that reproduces experimental barrier distribution values that give you an idea how to evaluate your theoretical calculations. Thus, you can compare your calculations and comment on the models you are considering. This method uses the least-squares method of the experimental cross section [25]. If the starting point is based on the classical fusion cross section, this method is briefly described as follows:

$$\sigma_{\mathrm{fus}}(E) = \pi R_{\mathrm{b}}^2 \left(1 - \frac{V_{\mathrm{b}}}{E}\right) \to E > V_{\mathrm{b}}\,, \qquad \sigma_{\mathrm{fus}}(E) = 0 \to E > V_{\mathrm{b}}\,. \tag{5}$$

The first derivative of $E\sigma_{\mathrm{fus}}$ is proportional to the classical penetration $T(E)$ for a one-dimensional barrier of height V_{b}, *i.e.* for $V_{\mathrm{b}} > E$ and $T(E) = 1$, $V_{\mathrm{b}} < E$, the second derivative is proportional to a delta function [29, 35, 38]

$$\frac{\mathrm{d}^2}{\mathrm{d}E^2}\left[E\sigma_{\mathrm{fus}}(E)\right] = \pi R_{\mathrm{b}}^2 \delta(E - V_{\mathrm{b}})\,. \tag{6}$$

$E\sigma_{\mathrm{fus}}$'s second derivative related to energy can give information about self-barriers. However, the transmission factor leads to a limited width for self-barriers [39]. Quantum tunneling was taken into account by Wong [40], who used Hill–Wheeler transmission coefficients [41] that apply when the barrier approaches with an inverted parabola to subtract the following expression for the fusion cross section in the barrier equation. Therefore, the derivative of equation $E\sigma_{\mathrm{fus}}$ may not lead to a clear definition of the individual self-barriers. Especially, for a poor connection situation, some of the Coulomb barriers are closely spaced. The Coulomb barrier distribution equation for

fusion is given as follows [29, 35, 38, 39]:

$$\frac{\mathrm{d}^2}{\mathrm{d}E^2}\left[E\sigma_{\mathrm{fus}}(E)\right] = \pi R_{\mathrm{b}}^2 \frac{2\pi}{\hbar w}\frac{\mathrm{e}^x}{1+\mathrm{e}^x} \tag{7}$$

$\hbar w$: barrier curvature $x = 2\pi\left(E - V_{\mathrm{b}}\right)/\hbar w$.

3. Results

O^{16}+$Ge^{70,72,74,76}$ reaction system

We systematically examined the fusion cross sections of O^{16}+$Ge^{70,72,74,76}$ reaction system with CCFULL, NRV coupled-channel codes and Wong's formalism in the energy range of 30–55 MeV-cm.

The projectile in these reactions includes different isotopes of germanium and the target nucleus is O^{16}. The nucleus has coupling vibrational states. The calculation parameters are given in Table I and Table II. The motivation for studying the Ge nucleus is that the nucleus has extremely interesting features that are exciting from both theoretical and experimental perspectives. The nucleus belongs to the weak deformation zone and is very shape unstable (soft). These softness properties have been proposed as a possible explanation for certain strange effects observed in sub-barrier [15]. These four systems were examined in the literature by Aguilera *et al.* [15], both experimentally and theoretically with the CCDEF coupled-channel calculation code [15]. It was observed that the results obtained from the CCFULL, NRV, and Wong's formula and the experimental data were compatible with the experimental data in the low- and high-energy regions, respectively. CCFULL and NRV use both the deformation parameters and excitation energies of the 2^+ and 3^- states for the target nucleus, while for the projectile nuclei, CCFULL uses only the 3^- state excitation energy and the deformation parameter.

TABLE I

Depth parameter V_0 and the surface diffuseness parameter a_0 [14].

System	V_0 [MeV]	a_0 [fm]
O^{16}+Ge^{70}	55.547	0.638
O^{16}+Ge^{72}	55.997	0.639
O^{16}+Ge^{74}	56.241	0.639
O^{16}+Ge^{76}	56.477	0.640

TABLE II

β_3^{N} values and the corresponding excitation energies of 3^- states of $Ge^{70,72,74,76}$ targets [14, 42, 43].

Target	β_3^{N}	Excitation energy [MeV]
Ge^{70}	0.274	2.561
Ge^{72}	0.264	2.515
Ge^{74}	0.145	2.536
Ge^{76}	0.144	2.692

The results of coupled-channel calculations, with codes and Wong's formula, are compared with the experimental data in Fig. 1 (a): CCFULL (black dashed), NRV (black dash-dotted), Wong's formalism (black solid line) and experimental data (black dotted), for the reactions of O^{16} projectile on Ge^{70} target, CCFULL (grey/blue star), NRV (grey/blue solid circle), Wong's formalism (grey/blue diamond) and experimental data (grey/blue circle) for the reactions of O^{16} projectile on Ge^{72} target; in Fig. 1 (b), the results with the same notification for the reactions of O^{16} projectile on $Ge^{74,76}$ targets are presented. It is worth noting that the results produced by these calculation models are close to each other and are in harmony with the experimental results at all energy scales. After all, it can be noticed that larger deformations below the barrier correspond to the large lower-barrier reinforcement of the fusion section and also that the fusion process is a tunnelling process under the barrier that can be added. These results show that the calculation models are realistic, so they can be used as a simulation to obtain the cross-section values to get a reliable idea. This confirms that these codes can be used to study the cross sections with the couplings between relative motion and internal degrees of freedom in heavy-ion fusion reactions. If the parameters are calculated carefully, the results that are most suitable for the experimental results are obtained with these models.

In Fig. 1 (c), the fusion barrier distribution calculated for coupling with CCFULL (Coupling) (black dotted line), Wong's formalism (black solid line), NRV (black solid circle) for the reaction of O^{16}+Ge^{70}, CCFULL (Coupling) (grey/blue dotted line), Wong's formalism (grey/blue solid line), NRV (grey/blue solid circle) for the reaction of O^{16}+Ge^{72} are shown. In Fig. 1 (d), the same assignments for the reactions of O^{16}+$Ge^{74,76}$ targets are presented. When we examined the results, we observed that the barrier distribution curves of the coupling we obtained in CCFULL and NRV were compatible with each other in four systems. It formed a single peak in the curve obtained from Wong's formula, and no fluctuation outside the barrier zone were derived. If we consider their relative positions and not the height of the peaks, then Wong's formula can be considered as a good method for extracting the experimental fusion cross section.

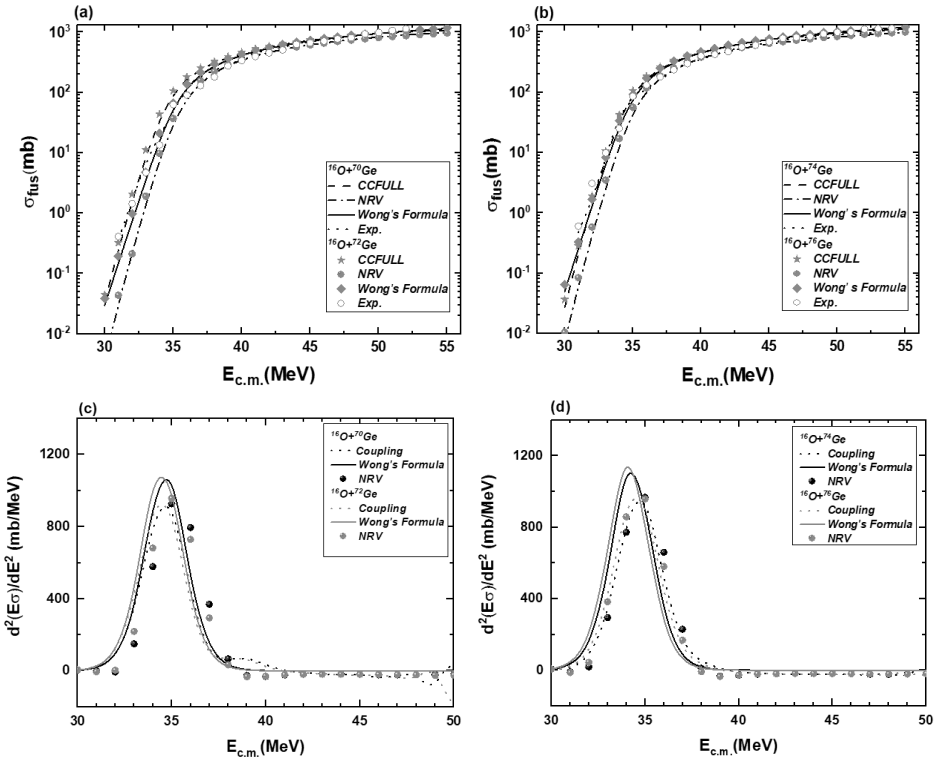

Fig. 1. (Colour on-line) (a), (b) Fusion excitation functions using CCFULL, NRV, Wong's formalism and experimental data for the reactions of O^{16} projectile on Ge^{70-76}targets; (c), (d) Barrier distribution calculations with CCFULL (coupled), Wong's formalism, NRV are shown.

O^{16}+$Sm^{148,150,152,154}$ reaction system

O^{16}+$Sm^{148,150,152,154}$ fusion excitation functions, taking the scattering potential as the sum of the Coulomb and the proximity potential, and using the one-dimensional barrier penetration model, were calculated in the 55–70 MeV-cm energy range by using CCFULL, NRV coupled-channel codes, Wong's formalism and compared with the experimental data [17] (see below). Figure 2 (a) presents fusion excitation functions of O^{16}+Sm^{148} with CCFULL (dashed line), NRV (dash-dotted line), Wong's formalism (solid line) with experimental data (dotted line); CCFULL (star), NRV (solid circle), Wong's formalism (diamond) with experimental data (circle) for the reaction of O^{16}+Sm^{150}, see also Fig. 2 (b) for fusion excitation functions for O^{16}+$Sm^{152,154}$.

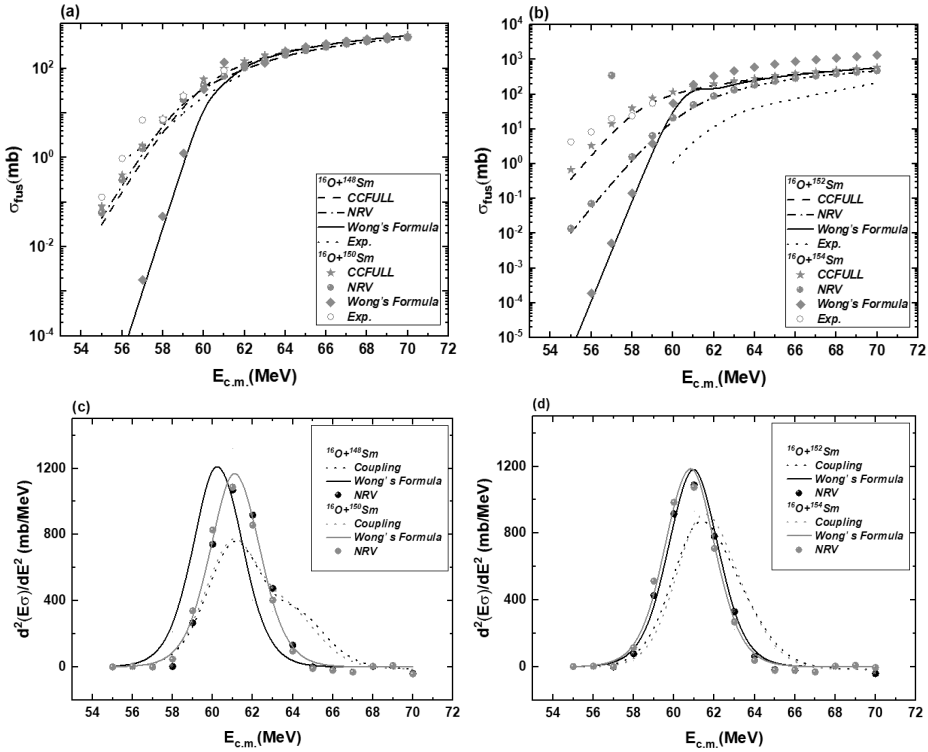

Fig. 2. (Colour on-line) (a) Fusion excitation functions of O^{16}+$Sm^{148,150}$; (b) Fusion excitation functions of O^{16}+$Sm^{152,154}$ with CCFULL, NRV, Wong's formalism with experimental data; (c) Barrier distributions for O^{16}+$Sm^{148,150}$; (d) Barrier distributions for O^{16}+$Sm^{152,154}$ with CCFULL (Coupling), NRV and Wong's formalism.

It should be noted that in the case of reactions, the target Sm nuclei show a wide range of deformation from the most stable spherical semi-magical Sm^{148} to well-deformed Sm^{154}. For single-phonon couplings in Sm^{148}, Sm^{150}, Sm^{152} and Sm^{154}, the β_3 values and the excitation energies of 3^- states are given in Table III, and for the reactions the potential and diffuseness parameters are given in Table IV. At and above the barrier, CCFULL, NRV and the simple one-dimensional barrier penetration model developed by Wong explain the fusion reactions of heavy-ions very well, while using the scattering potential as the sum of Coulomb and proximity potentials. Larger deformations below the barrier correspond to a large lower-barrier strengthening of the fusion sections.

The total width of the barrier distribution is presented in Fig. 2 (c) with barrier distributions with CCFULL (Coupling) (black dotted line), NRV (black solid circle) and Wong's formalism (black solid line) for O^{16}+Sm^{148}, CCFULL (Coupling) (grey/blue dotted line), NRV (grey/blue solid circle)

TABLE III

β_3^{N} values and the corresponding excitation energies of 3^- states of $\mathrm{Sm}^{148,150,152,154}$ targets [14, 42, 43].

Target	β_3^{N}	Excitation energy [MeV]
Sm^{148}	0.158	1.162
Sm^{150}	0.145	1.071
Sm^{152}	0.095	1.041
Sm^{154}	0.080	1.012

TABLE IV

Depth parameter V_0 and the surface diffuseness parameter a_0 [14].

System	V_0 [MeV]	a_0 [fm]
$\mathrm{O}^{16}+\mathrm{Sm}^{148}$	62.200	0.652
$\mathrm{O}^{16}+\mathrm{Sm}^{150}$	62.320	0.652
$\mathrm{O}^{16}+\mathrm{Sm}^{152}$	62.420	0.652
$\mathrm{O}^{16}+\mathrm{Sm}^{154}$	62.530	0.652

and Wong's formalism (grey/blue solid line) for $\mathrm{O}^{16}+\mathrm{Sm}^{150}$. Figure 2 (d) presents the same assignments as with Fig. 2 (c) for $\mathrm{O}^{16}+\mathrm{Sm}^{152,154}$. The figures suggest that the coupling between consecutive members of a collective band is important in these reactions. It appears that the data can be well-represented using the deformation parameters accepted in our calculations, provided that expected weak couplings are included. It is also possible that the more realistic coupling option between several members of a vibratory band can produce similar properties. Also, if we want to decrease the width of the distribution curves, we need to increase the number of channels.

$\mathbf{Ne^{20}+Zr^{90,92,94,96}}$ reaction system

We examined the fusion cross sections of the $\mathrm{Ne}^{20}+\mathrm{Zr}^{90,92,94,96}$ reactions system with CCFULL, NRV coupled-channel codes and Wong's formalism in the 40–80 MeV-cm energy range with the parameters given in Table V and

TABLE V

Depth parameter V_0 and the surface diffuseness parameter a_0 [14].

System	V_0 [MeV]	a_0 [fm]
$\mathrm{Ne}^{20}+\mathrm{Zr}^{90}$	61.548	0.651
$\mathrm{Ne}^{20}+\mathrm{Zr}^{92}$	61.760	0.651
$\mathrm{Ne}^{20}+\mathrm{Zr}^{94}$	61.967	0.651
$\mathrm{Ne}^{20}+\mathrm{Zr}^{96}$	62.170	0.652

Table VI. There is no experimental or theoretical study in the literature for these systems. Our aim to study these reactions is to contribute to the literature by producing theoretical data for reactions in the absence of experimental data. The data obtained from NRV for Zr isotopes at below the barrier potential parameters remained far from the harmony parallelism in the scale (see Fig. 3 (a) and (b)).

TABLE VI

β_3^{N} values and the corresponding excitation energies of 3^- states of $Zr^{90,92,94,96}$ targets [14, 42, 43].

Target	β_3^{N}	Excitation energy [MeV]
Zr^{90}	0.211	2.748
Zr^{92}	0.174	2.340
Zr^{94}	0.193	2.058
Zr^{96}	0.284	1.897

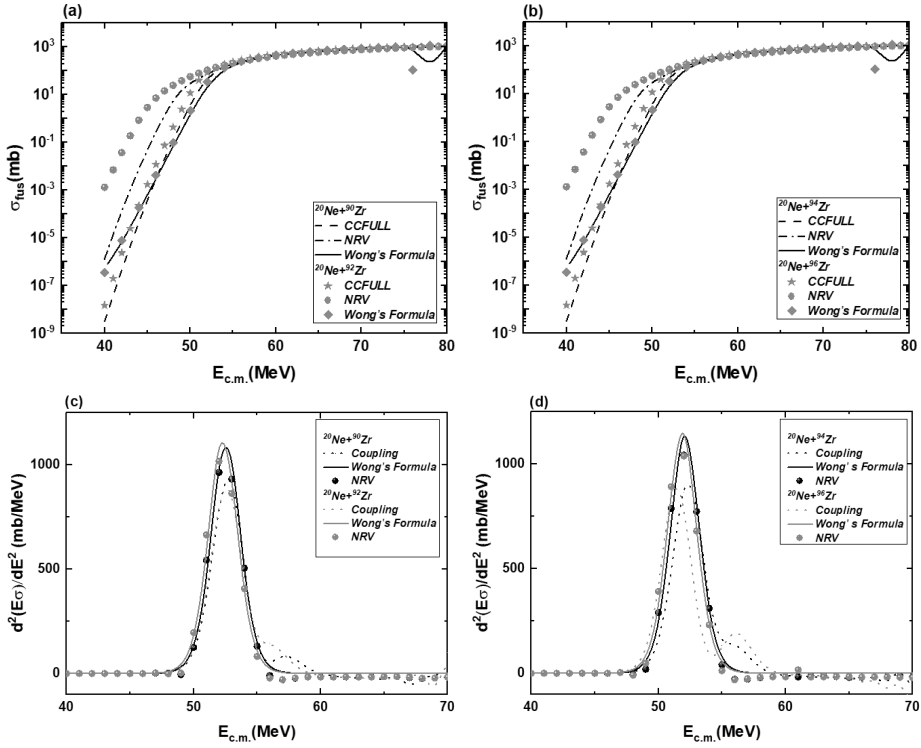

Fig. 3. (Colour on-line) (a), (b) Fusion excitation functions for the reactions of Ne^{20} projectile on $Zr^{90,92,94,96}$ targets; (c), (d) Barrier distribution calculations are shown.

Figure 3 (a) presents fusion cross sections of Ne^{20}+Zr^{90} with CCFULL (dashed line), NRV (dash-dotted line), Wong's formalism (solid line); CCFULL (star), NRV (solid circle), Wong's formalism (diamond) for the reaction of Ne^{20}+Zr^{92}. Figure 3 (b) shows the results with the same assignments for Ne^{20}+$Zr^{94,96}$. We observed that when we reached the barrier parameters and exceeded these parameters, the results we obtained from all codes and Wong's formalism progressed on the same scale. Barrier distributions for Ne^{20}+$Zr^{90,92,94,96}$ reactions are given in Fig. 3 (c) and Fig. 3 (d): barrier distributions with CCFULL (Coupling) (black dotted line), NRV (black solid circle) and Wong's formalism (black solid line) for Ne^{20}+$Zr^{90,94}$, CCFULL (Coupling) (grey/blue dotted line), NRV (grey/blue solid circle) and Wong's formalism (grey/blue solid line) for Ne^{20}+$Zr^{92,96}$. Approximately the same distribution was observed for all isotopes of Zr. Coupling revealed two peaks, NRV a single peak, and Wong's formula revealed a single peak. A potential change is required to eliminate the dispersion deviation seen in coupling.

Ne^{20}+$Sn^{112,114,116,118,120}$ reaction system

The fusion cross sections of the Ne^{20}+$Sn^{112,114,116,118,120}$ reaction systems were investigated with CCFULL, NRV coupled-channel codes and Wong's formalism in the energy range of 60–100 MeV-cm with parameters given in Table VII. The aim was to obtain information about the fusion cross sections of these reactions. Barrier parameter values for $A = 112$, 114, 116, 118, 120 in the target core were determined as 63.643 MeV, 63.810 MeV, 63.975 MeV, 64.137 MeV, 64.295 MeV, respectively (Table VIII).

TABLE VII

β_3^{N} values and the corresponding excitation energies of 3^- states of $Sn^{112,114,116,118,120}$ targets [14, 42, 43].

Target	β_3^{N}	Excitation energy [MeV]
Sn^{112}	0.128	2.355
Sn^{114}	0.134	2.275
Sn^{116}	0.152	2.266
Sn^{118}	0.139	2.325
Sn^{120}	0.137	2.401

TABLE VIII

Depth parameter V_0 and the surface diffuseness parameter a_0 [14].

System	V_0 [MeV]	a_0 [fm]
Ne^{20}+Sn^{112}	63.643	0.655
Ne^{20}+Sn^{114}	63.810	0.655
Ne^{20}+Sn^{116}	63.975	0.655
Ne^{20}+Sn^{118}	64.137	0.655
Ne^{20}+Sn^{120}	64.295	0.655

When we examined the data obtained with this information, we observed that all codes in the studied energy range were in very good harmony with each other, except for the region just below the barrier (see Fig. 4 (a)); CC-

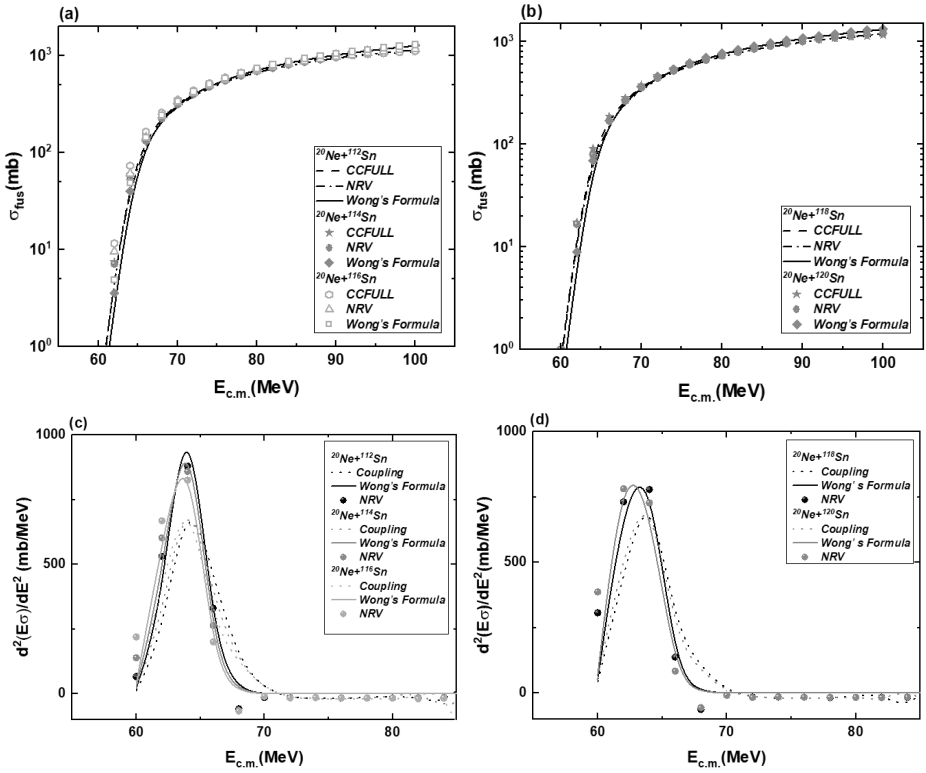

Fig. 4. (Colour on-line) (a), (b) The comparison of the computed fusion cross sections of Ne^{20}+$Sn^{112,114,116,118,120}$ with CCFULL, NRV, Wong's formalism with experimental data; (c), (d) Barrier distributions with CCFULL (Coupling), NRV and Wong's formalism for the reaction system.

FULL (black dashed line), NRV (black dash-dotted line), Wong's formalism (black solid line) for Ne^{20}+Sn^{112}; CCFULL (grey/blue star), NRV (grey/blue solid circle), Wong's formalism (grey/blue diamond) for Ne^{20}+Sn^{114}, CCFULL (light grey/green circle), NRV (light grey/green up-triangle), Wong's formalism (light grey/green square) for Ne^{20}+Sn^{116}. In Fig. 4 (b), the results with the same assignments are shown for Ne^{20}+$Sn^{118,120}$ with $Sn^{112,114}$. We plotted a comparison of the barrier distributions for Ne^{20}+$Sn^{112,114,116,118,120}$ with calculations performed using the CCFULL coupled-channel code (Coupling), NRV code, and Wong's formula. Figure 4 (c) presents barrier distributions with CCFULL (Coupling) (black dotted line), NRV (black solid circle) and Wong's formalism (black solid line) for Ne^{20}+Sn^{112}; the results with the same assignments for Ne^{20}+Sn^{114} with grey/blue colour and for Ne^{20}+Sn^{116} with light grey/green colour. Figure 4 (d) presents BDs with CCFULL (Coupling) (black dotted line), NRV (black solid circle) and Wong's formalism (black solid line) for Ne^{20}+Sn^{118}. The BDs are presented with the same assignments for Ne^{20}+Sn^{120} and marked with grey/blue colour. The shapes of the distributions show some isotopic effects. More importantly, a comparison between coupling (NRV, CCFULL) and Wong's formalism for the five-reaction group differs in that the calculations are much more structured than Wong's formula. Coupling-NRV curves obtained by coupled-channel codes showed consistent distributions in the barrier region.

Si^{28}+$Mg^{24,26}$ reaction system

In Fig. 5 (a), the data obtained as a result of fusion cross-section calculations made with CCFULL code, NRV code and Wong's formula are plotted. The CCFULL coupling curve is represented by dotted line, NRV by dash-dotted line, Wong's formula by solid line and the experimental data by dotted line for Si^{28}+Mg^{24} and CCFULL as star, NRV as solid circle, Wong's formula as diamond, the experimental data as circle. The experimental data has been taken from Ref. [18].

$Mg^{24,26}$ and Si^{28} nuclei are deformed and have to be rotators. By taking into account this property of the projectile and treating the target as an inert nucleus, we obtain good harmony between theoretical predictions with coupled-channel calculations and experimental data both for cross sections and for the barrier distributions (see Fig. 5 (a) and Fig. 5 (b)). The interaction potentials were chosen in the Akyüz–Winther form, and they are displayed in Table IX and Table X. The fusion barrier height for Si^{28}+Mg^{24} equals 25.03 MeV, the radius parameter is 1.16 fm and for Si^{28}+Mg^{26}, V_0 = 24.70 MeV and r_0 = 1.17 fm. According to the obtained results, we observed that the closest results to the experimental ones in the low-energy region are in compliance with the CCFULL code, and when we come to the barrier zone, the results obtained from the NRV and Wong's formula

are in agreement with the experimental data. In Fig. 5 (b), the graph of the data of fusion barrier distributions for the defined reaction is presented. The graph shows the fusion barrier distribution (with CCFULL and NRV) calculated for coupling and the calculation results using Wong's formula. It can be seen that the distributions of the couples get closer to each other and that they have the same parallelism in the distribution with the scale obtained with Wong's formula. NRV and Wong's formula may need a little oscillation in potential around 24 MeV to get the peak at the same energy with the coupling curve.

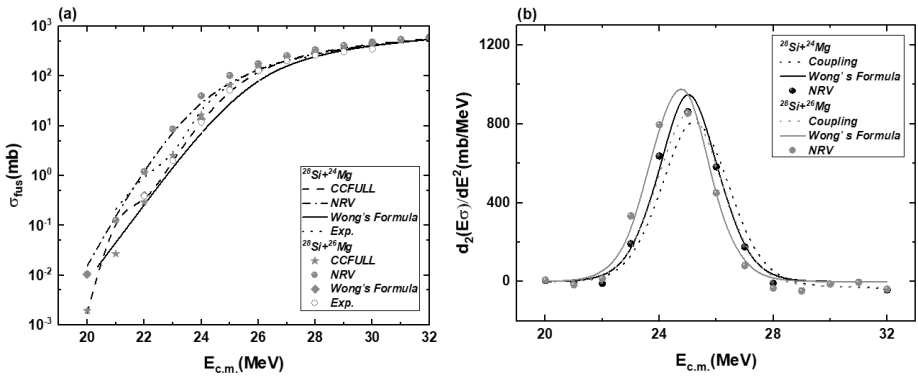

Fig. 5. (a) Fusion cross section for Si^{28}+$Mg^{24,26}$ reaction system with CC calculations using CCFULL, NRV and Wong's formula; (b) The fusion barrier distribution for the same system.

TABLE IX

Depth parameter V_0 and the surface diffuseness parameter a_0 [14].

System	V_0 [MeV]	a_0 [fm]
Si^{28}+Mg^{24}	51.987	0.629
Si^{28}+Mg^{26}	52.906	0.632

TABLE X

β_3^{N} values and the corresponding excitation energies of 3^- states of $Mg^{24,26}$ targets [14, 42, 43].

Target	β_3^{N}	Excitation energy [MeV]
Mg^{24}	0.326	7.616
Mg^{26}	0.213	6.876

Si^{28}+$Ni^{58,64}$ reaction system

The fusion cross-section calculations for the Si^{28}+$Ni^{58,64}$ reactions were investigated in the 40–75 MeV-cm energy range with CCFULL, NRV coupled-channel codes and Wong's formula and plotted in Fig. 6 (a): CCFULL (dashed line), NRV (dash-dotted line), Wong's formula (solid line) and the experimental data (dotted line) for Si^{28}+Ni^{58} and CCFULL (star), NRV (solid circle), Wong's formula (diamond), the experimental data (circle) for Si^{28}+Ni^{64}.

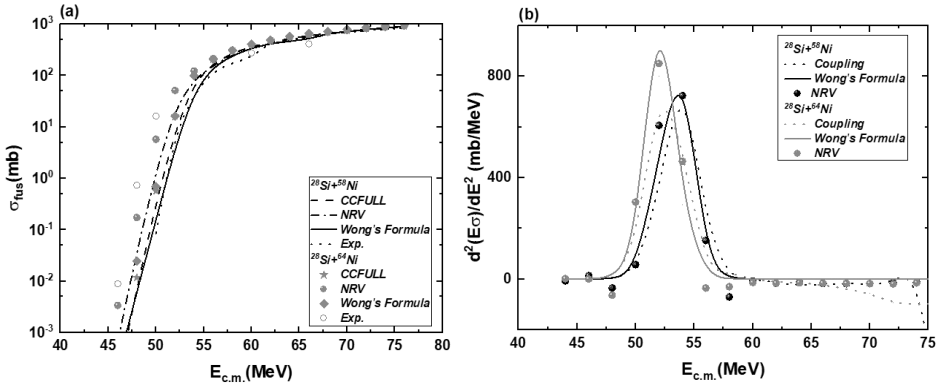

Fig. 6. (a) Fusion cross sections of Si^{28}+$Ni^{58,64}$ with CC calculations using CCFULL, NRV and Wong's formula; (b) Fusion barrier distribution for the same system.

The coupling cross section taken as the projectile is a rotator and the target is an inert mode. The Akyüz–Winther parameters, which provide the most optimal results for this barrier, and excitation parameters for the target are listed in Table XI and Table XII. Experimental cross-section data are taken from Stefanini *et al.* [19]. The motivation to study this reaction is that there is no theoretical study in the literature on the coupled-channel codes covered by this work. The compatibility of cross sections between the codes is shown in Fig. 6 (a). Figure 6 (b) shows the calculated fusion barrier distribution for coupling with CCFULL (dotted line), NRV (circle), and the calculated using Wong's formula (solid line).

The coupling curve shows almost the same behaviour as the fusion barrier distribution in NRV and the results obtained from the calculation method with Wong's formula, but it draws attention with little difference. Therefore, for this system, it can be concluded that the fusion process is greatly affected by both the projectiles and that the target nuclei are excited from low levels. Distribution curves show the same behaviour in all calculations, giving reliable results in the absence of experimental barrier distributions.

TABLE XI

Depth parameter V_0 and the surface diffuseness parameter a_0 [14].

System	V_0 [MeV]	a_0 [fm]
Si^{28}+Ni^{58}	62.128	0.652
Si^{28}+Ni^{64}	63.25	0.654

TABLE XII

β_3^{N} values and the corresponding excitation energies of 3^- states of $Ni^{58,64}$ targets [14, 42, 43].

Target	β_3^{N}	Excitation energy [MeV]
Ni^{58}	0.198	4.475
Ni^{64}	0.201	3.56

Si^{28}+$Zr^{90,92,94,96}$ reaction system

For Si^{28}+$Zr^{90,92,94,96}$ systems, we calculated the fusion cross sections around the Coulomb barrier with CCFULL, NRV codes and Wong's formalism and the results are presented in Fig. 7 (a) and Fig. 7 (b). Figure 7 (a) presents the fusion cross-section calculations of Si^{28}+Zr^{90} with CCFULL (black dashed line), NRV (black dash-dotted line), Wong's formula (black solid line) and experimental values (black dotted line) [20], and CCFULL (grey/blue star), NRV (grey/blue solid circle) and experimental data (grey/blue circle) for Si^{28}+Zr^{92}. Figure 7 (b) presents the fusion cross-section calculations of Si^{28}+Zr^{94} with CCFULL (black dashed line), NRV (black dash-dotted line), Wong's formula (black solid line) and experimental values (black dotted line), and CCFULL (grey/blue star), NRV (grey/blue solid circle) and Wong's formula (grey/blue diamond) for Si^{28}+Zr^{96}.

The ion–ion potentials used in these calculations are the Woods–Saxon parameters of the Akyüz–Winther potential given in Table XIII, and the deformation parameters and excitation energies for vibrational modes 3^- of the target are given in Table XIV.

TABLE XIII

Depth parameter V_0 and the surface diffuseness parameter a_0 [14].

System	V_0 [MeV]	a_0 [fm]
Si^{28}+Zr^{90}	67.009	0.661
Si^{28}+Zr^{92}	67.345	0.662
Si^{28}+Zr^{94}	67.585	0.662
Si^{28}+Zr^{96}	67.820	0.662

TABLE XIV

β_3^{N} values and the corresponding excitation energies of 3^- states of $Zr^{90,92,94,96}$ targets [14, 42, 43].

Target	β_3^{N}	Excitation energy [MeV]
Zr^{90}	0.211	2.748
Zr^{92}	0.174	2.340
Zr^{94}	0.193	2.058
Zr^{96}	0.284	1.897

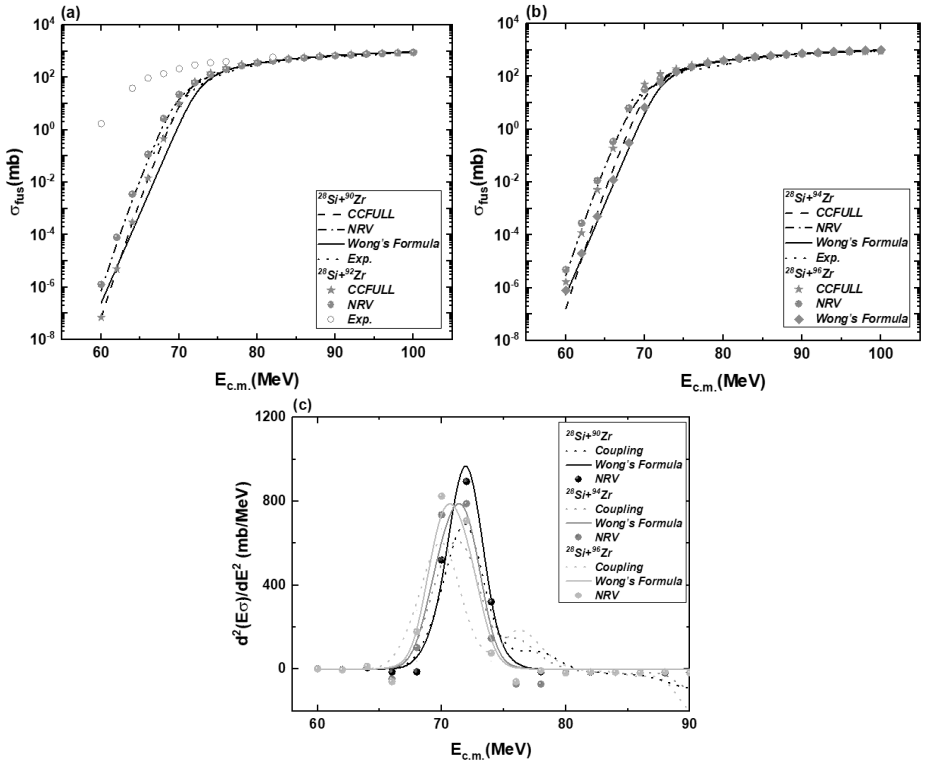

Fig. 7. (Colour on-line) (a) Fusion cross sections of $Si^{28}+Zr^{90,92,94,96}$ with CC calculations using CCFULL, NRV and Wong's formula; (b) Fusion barrier distribution for the $Si^{28}+Zr^{90,94,96}$system.

For the reaction systems, when the theoretically calculated cross sections are evaluated in the lower barrier region, the CCFULL, NRV and Wong calculations are larger in order of magnitude compared to experimental data of Zr^{92}. On the other hand, in parameters of the magnitude that we approached and exceeded the barrier zone, all codes gave results compatible

with each other. The reaction system was studied experimentally by Kalkal *et al.* and the experimental data were presented in the literature [20]. In the same study they made calculations with CCFULL code. We have observed that the calculation models give results that are compatible with both theoretical and experimental data. All calculations are reliable in the absence of experimental data for this reaction group or in environments where there are no suitable conditions for experimentation. Figure 7 (c) shows the barrier distributions for defined reactions, for Si^{28}+Zr^{90}: CCFULL (Coupling) (black dotted line), Wong's formula (black solid line), NRV (black solid circle); for Si^{28}+Zr^{94}: CCFULL (Coupling) (grey/blue dotted line), Wong's formula (grey/blue solid line), NRV (grey/blue solid circle) and for Si^{28}+Zr^{96}: CCFULL (Coupling) (light grey/green dotted line), Wong's formula (light grey/green solid line), NRV (light grey/green solid circle). For the coupling used the CCFULL version, allowed the inclusion of two excited states in the target nuclei and one in the projectile, with the option to include multi-nuclei or omnidirectional states. As can be seen from the graph, all calculations gave a peak with the same distribution; they are suitable calculations to obtain reliable barrier distribution data.

Si^{28}+$Mo^{94,100}$ reaction system

The data observed with calculation methods (potential parameters and excitation parameters) given in Table XV and Table XVI were compatible with the experimental data on the entire energy scale.

TABLE XV

Depth parameter V_0 and the surface diffuseness parameter a_0 [14].

System	V_0 [MeV]	a_0 [fm]
Si^{28}+Mo^{94}	67.585	0.662
Si^{28}+Mo^{100}	68.274	0.663

TABLE XVI

β_3^{N} values and the corresponding excitation energies of 3^- states of $Mo^{94,100}$ targets [14, 42, 43].

Target	β_3^{N}	Excitation energy [MeV]
Mo^{94}	0.153	2.534
Mo^{100}	0.218	1.908

Fusion cross sections for selected systems were calculated using CCFULL, NRV codes and Wong's formalism, and the data were compared in Fig. 8 (a) with experimental results [12]: CCFULL (dashed line), NRV (dash-dotted line), Wong's formula (solid line) and the experimental data (dotted line) for Si^{28}+Mo^{94} and CCFULL (star), NRV (solid circle), Wong's formula (diamond) and the experimental data (circle) for Si^{28}+Mo^{100}.

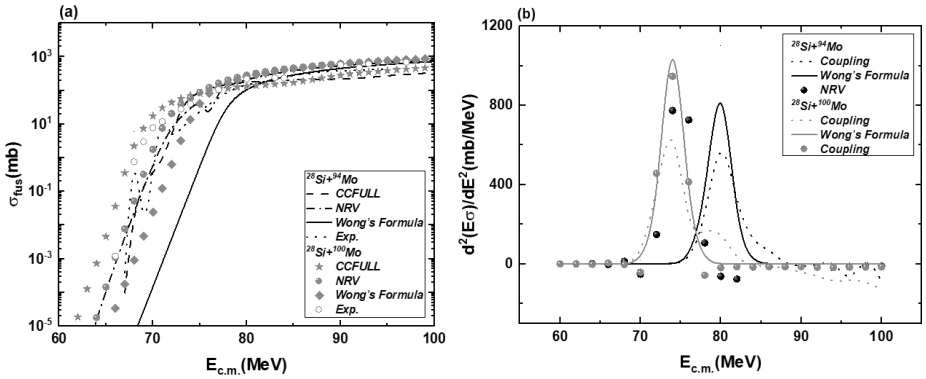

Fig. 8. (a) The comparison of the computed fusion cross sections of Si^{28}+$Mo^{94,100}$ with CCFULL, NRV, Wong's formalism with experimental data; (b) Barrier distributions with CCFULL (Coupling), NRV and Wong's formalism for the reaction system.

A phonon excitation of the lowest 2^+ and 3^- states of the target nucleus and the projectile was included in the calculation. In addition to the theoretical study, the experimental study of these two reactions working with the coupled-channel method was built by Ackermann *et al.* [21]. In Fig. 8 (b), the fusion barrier distribution functions of the systems are illustrated.

The coupling distributions in both reactions showed small peaks after exceeding the barrier energy. In order to prevent these small distributions, a deeper potential change for the potential region in question is required to avoid deviations of the distributions. When we look at 90 MeV and above, in the cross-section data, the CCFULL falls below the axis of harmony, and we see distortions in the same energy region in the distribution.

S^{32}+$Zr^{90,96}$ reaction system

Following the study of Zhang *et al.* [22] in which the reaction group was examined both experimentally and with CCDEF, which is one of the coupled-channel codes, the same reaction group was dealt with theoretically again in the 65–100 MeV-cm energy range (using the parameters given in Table XVII and Table XVIII), including different calculation methods, as CCFULL, NRV codes and Wong's formalism. Figure 9 (a) shows fusion cross-section results:

TABLE XVII

Depth parameter V_0 and the surface diffuseness parameter a_0 [14].

System	V_0 [MeV]	a_0 [fm]
$S^{32}+Zr^{90}$	69.345	0.665
$S^{32}+Zr^{96}$	70.107	0.666

TABLE XVIII

β_3^{N} values and the corresponding excitation energies of 3^- states of $Zr^{90,96}$ targets [14, 42, 43].

Target	β_3^{N}	Excitation energy [MeV]
Zr^{90}	0.211	2.748
Zr^{96}	0.284	1.897

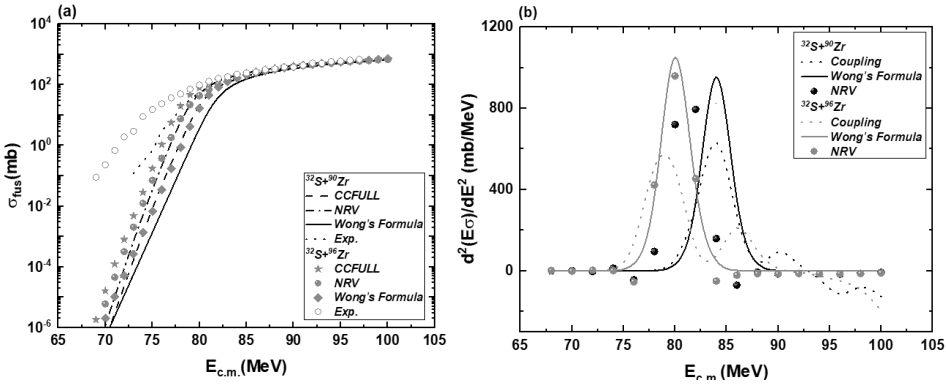

Fig. 9. (a) Fusion cross sections of $S^{32}+Zr^{90,96}$ with CC calculations using CCFULL, NRV and Wong's formula; (b) Fusion barrier distribution for the same system.

CCFULL (dashed line), NRV (dash-dotted line), Wong's formula (solid line) and the experimental data (dotted line) for $S^{32}+Zr^{90}$ and CCFULL (star), NRV (solid circle), Wong's formula (diamond), the experimental data (circle) for $S^{32}+Zr^{96}$. Fusion enhancement caused by static deformations and surface vibrations of the nuclei is well-defined in these coupled-channel calculations. Here, concordant data were obtained for the measurement results of the experimental fusion stimulation functions at and above the barrier parameters level, performed with small energy steps and with good statistical accuracy. The figure shows comparison of experimental fusion stimulation functions and CC calculations. The fusion excitation functions for near and above the Coulomb barrier have been calculated with fairly good accuracy.

Barrier distributions are presented in Fig. 9 (b). While a good peak is observed in the barrier dispersion potential for coupling, the NRV and Wong's results have moved away from this point and gave scattered peaks, the dispersion may disappear by changing the parameter. Small oscillations of coupling curves above 85 MeV and 90 MeV indicate a need for a deeper potential.

S^{36}+$Pb^{204,206,208,210}$ reaction system

The cross sections are well-reproduced in the reactions using Pb^{204}, Pb^{206}, Pb^{208} and Pb^{210} target nuclei, even at the lowest measured energies, when coupling to the first 2^+ and 3^- states of the sulfur and lead nuclei, respectively, is included. Energy and deformation of the 3^- states in Pb^{204}, Pb^{206}, Pb^{208} and Pb^{210} vary only smoothly. The parameters are listed in Table XIX and Table XX (V_0 and a_0).

TABLE XIX

Depth parameter V_0 and the surface diffuseness parameter a_0 [14].

System	V_0 [MeV]	a_0 [fm]
S^{36}+Pb^{204}	78.074	0.683
S^{36}+Pb^{206}	78.057	0.684
S^{36}+Pb^{208}	78.041	0.684
S^{36}+Pb^{210}	78.026	0.684

TABLE XX

β_3^N values and the corresponding excitation energies of 3^- states of $Pb^{204,206,208,210}$ targets [14, 42, 43].

Target	β_3^N	Excitation energy [MeV]
Pb^{204}	0.118	2.621
Pb^{206}	0.116	2.648
Pb^{208}	0.111	2.615
Pb^{210}	0.089	1.879

Fusion cross sections were obtained by using the CCFULL, NRV coupled-channel codes and Wong's formalism in the 135–175 MeV-cm energy range and compared with experimental data [23]. The results of the CC calculations are shown in Fig. 10 (a) and Fig. 10 (b). The calculated values for S^{36}+Pb^{204} are given in Fig. 10 (a) with CCFULL (black dashed line), NRV (black dash-dotted line), Wong's formula (black solid line) and experimental data (black dotted line); for S^{36}+Pb^{206}: CCFULL (grey/blue star), NRV (grey/blue solid circle), Wong's formula (grey/blue diamond), and experimental data (grey/blue circle). S^{36}+Pb^{208} and S^{36}+Pb^{210} reactions are

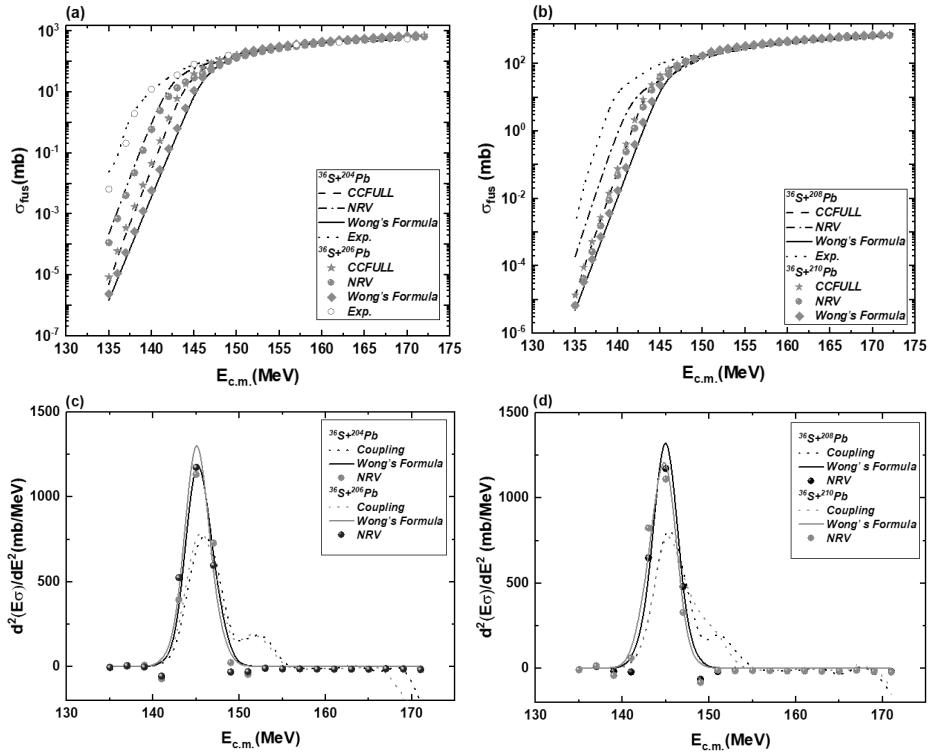

Fig. 10. (Colour on-line) (a) Fusion cross sections of S^{36}+$Pb^{204,206,208,210}$ with CCFULL, NRV, Wong's formalism with experimental data; (b) Barrier distributions with CCFULL (Coupling), NRV and Wong's formalism for the reaction system.

shown in Fig. 10 (b). S^{36}+Pb^{208} reaction is graphed with the same symbols as S^{36}+Pb^{204} reaction given in Fig. 10 (a), and S^{36}+Pb^{210} reaction is graphed with the same symbols as S^{36}+Pb^{206} reaction given in Fig. 10 (a). Each code gave results compatible with each other on the barrier energy and above, but the code that produced the closest results to the experimental results in the region close to the barrier was NRV. This may be due to a combination of more vibratory states or an increased softness in the input channel. Barrier distributions for S^{36}+$Pb^{204,206,208,210}$ reactions were calculated by coupling (CCFULL), NRV and Wong's formula, and the calculations were shown in Fig. 10 (c) and Fig. 10 (d). For S^{36}+$Pb^{204,208}$ the calculation results are shown as coupling (black dotted line), Wong's formula (black solid line) and NRV (black solid circle), and for S^{36}+$Pb^{206,210}$, the results are shown with the same assignments in grey/blue colour. In barrier distribution calculations (CCFULL and NRV), the lowest states, *i.e.* 2^+ and 3^- states, are plotted for all reactions. While a peak with full barrier potential value was observed in all reactions for three calculations, a small and unde-

sirable peak was observed after passing the barrier in calculations made with CCFULL. In order to decrease the width of the distribution curve, the number of channels should be increased, and the potential parameter should be increased to eliminate the small peaks that appear after passing the barrier potential.

Ar^{40}+$Hf^{176,178,180}$ reaction system

The fusion cross sections with coupled-channel calculations (CCFULL, NRV codes) and Wong's formalism for Ar^{40}+$Hf^{176,178,180}$ reactions were compared with the experimental data [24] in Fig. 11 (a): CCFULL (black dashed line), NRV (black dash-dotted line), Wong's formalism (black solid line), experimental data (black dotted line) for Ar^{40}+Hf^{176}; CCFULL (grey/blue star), NRV (grey/blue solid circle), Wong's formalism (grey/blue diamond), experimental data (grey/blue circle) for Ar^{40}+Hf^{178}; CCFULL (light grey/green hexagonal), NRV (light grey/green circle), Wong's formalism (light grey/green up-triangle) and experimental data (light grey/green square) for Ar^{40}+Hf^{180}. In the coupled-channel calculations, the lines represent calculations of vibrational modes in the projectile and target nucleus.

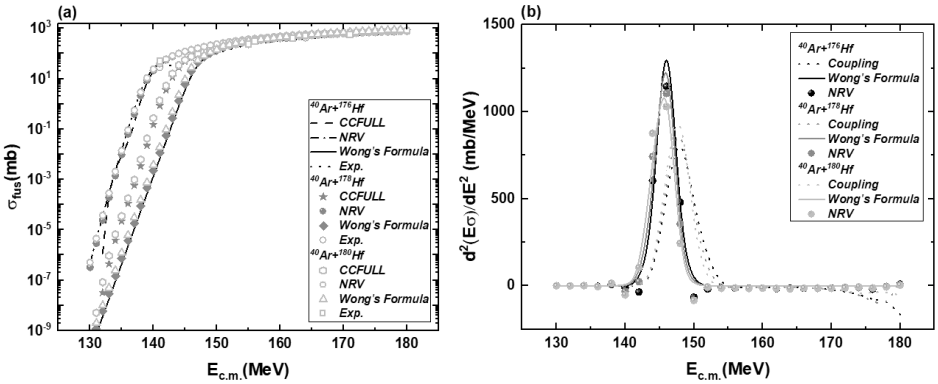

Fig. 11. (Colour on-line) (a) Fusion cross sections of Ar^{40}+$Hf^{176,178,180}$ with CC calculations using CCFULL, NRV and Wong's formula; (b) Fusion barrier distribution for the same system.

Depth parameter V_0 and surface diffusion parameter a_0 (Wood–Saxon potentials) were calculated and the values are shown in Table XXI. The codes contain the lowest states for all reactions, *i.e.* 2^+ and 3^- states (3^- states of target nuclei, see Table XXII). The calculated cross sections are in good agreement with the experimental data. If the parameters are calculated meticulously, the data that best suits the experimental result are obtained with these codes.

TABLE XXI

Depth parameter V_0 and the surface diffuseness parameter a_0 [14].

System	V_0 [MeV]	a_0 [fm]
Ar^{40}+Hf^{176}	79.015	0.684
Ar^{40}+Hf^{178}	79.015	0.684
Ar^{40}+Hf^{180}	79.017	0.684

TABLE XXII

β_3^{N} values and the corresponding excitation energies of 3^- states of $Hf^{176,178,180}$ targets [14, 42, 43].

Target	β_3^{N}	Excitation energy [MeV]
Hf^{176}	0.057	1.313
Hf^{178}	0.044	1.322
Hf^{180}	0.026	1.374

The fusion barrier distribution calculations (coupling, NRV, Wong's formula) are plotted in Fig. 11 (b). BDs for defined reactions for Ar^{40}+Hf^{176}: CCFULL (black dotted line), Wong's formula (black solid line), NRV (black solid circle); for Ar^{40}+Hf^{178}: CCFULL (grey/blue dotted line), Wong's formula (grey/blue solid line), NRV (grey/blue solid circle) and for Ar^{40}+Hf^{180}: CCFULL (light grey/green dotted line), Wong's formula (light grey/green solid line), NRV (light grey/green solid circle). While the data for NRV calculation shows the peak in the barrier potential in the expected region (barrier heights are 148.35 MeV, 148.01 MeV, 147.68 MeV, respectively), the coupling curve obtained with CCFULL and Wong remained slightly away from the region. By changing the potential parameter, the curve region can be shifted back and harmony between calculations can be achieved.

4. Conclusions

There is much discussion about the need to use coupled-channel method to generate fusion cross-section data. Given the same sets of nuclear potential parameters, several programs are available that use their unique methods to calculate the same fusion cross sections. Until now, heavy-ion fusion reactions have been experimentally and theoretically approached, using one or two of these codes, fusion cross sections have been calculated, and the accuracy of the coupled-channel code/codes used has been examined by comparing with the existing experimental data. The aim was to fit the fu-

sion cross-section values into experimental data by changing the parameters used in the codes. In this study, fusion cross-section calculations were made using CCFULL, NRV coupled-channel codes and Wong's formalism for selected reactions, their comparisons with experimental fusion cross sections were graphically presented, the code or the codes that gave the best results when compared with the experimental data were determined, and also the differences between the codes were determined. The codes use the scattering potential as the sum of the Coulomb and proximity potentials, and each coupled-channel code calculates as vibrational couplings in the reacting nuclei. The models applied in these two codes (CCFULL and NRV) are nearly the same. In accordance with the purpose of the study, the reactions were studied with CCFULL and NRV, and it was shown with the obtained results that although the mathematical (numerical) realizations in CCFULL and NRV calculations are different in some details, the algorithms are close. Another noticeable difference between these two codes is the way of calculating the matrix element. NRV implements a more accurate scheme for matrix element calculation [2, 33].

It should be noted that the results are in good agreement with the experimental data on the scales. As a result, it was realized that larger deformations below the barrier correspond to the large lower-barrier reinforcement of the fusion section, and it can be added that the fusion process is a tunneling process under the barrier.

The most important aim of the study is to obtain instructive data for reactions that have no experimental data. It has been demonstrated and verified that researchers who want to theoretically examine fusion cross sections in areas where experimental conditions cannot be met can use both CCFULL and NRV to obtain reliable data as a simulation. This confirms that these codes can be used in heavy-ion fusion reactions to examine cross sections with relationships between relative motion and internal degrees of freedom. If the parameters are calculated carefully, it is possible to obtain the closest results to the experimental data for other investigations with these codes. In Si^{28}+$Mo^{94,100}$, Ar^{40}+Hf^{178}, and S^{32}+Zr^{90} reactions, we have encountered a shallow potential warning. Potentials such as the Akyüz–Winther (AW) provide reliable barriers, but they cannot generate the data far below the barrier, and the ion–ion potential barrier must have another form inside. After a series of simple but obvious arguments, it is thought that the exponential decrease in tunnelling probability may be related to the loss of the classically allowed region below certain energy. If this is true then there is a shallow pocket of potential within the barrier.

The concept of barrier distribution is useful for studying the effect of the structure of the nuclei involved in the reaction. We performed coupled-channel analysis for fusion barrier distribution to investigate the character-

istic features of the structure of selected isotopes proposed by the Coulomb excitation experiments. There are several theoretical approaches to examine fusion barrier distributions. In this study, the modified version of CCFULL code (Coupling), NRV code with theoretical aspect and second derivate of Wong's formula for fusion cross section to extract BDs from experimental data are used for barrier distributions. The fusion barrier distribution obtained by the Wong formula is a proportional way of determining the number of effective barriers resulting from channel coupling effects for inducing interactive nuclei. From the comparison, we conclude that CCFULL and NRV are the foolproofing calculation codes for generating the data of the fusion barrier distribution, and the second derivate of Wong's formula produced acceptable BDs data when compared with theoretical calculations. The inclusion of coupling effects for full quantum mechanical calculations, considering the vibrational deformations, increases the computations below and above the Coulomb barrier, but the region under the Coulomb barrier is the best fit, especially in deriving the data.

REFERENCES

[1] K.P. Santhosh, V. Bobby Jose, «Heavy-ion fusion reactions of ^{16}O on spherical/deformed $^{144-154}$Sm targets using Coulomb and proximity potentials», *Rom. Rep. Phys.* **66**, 939 (2014), `http://rrp.infim.ro/2014_66_4/A3.pdf`

[2] K. Hagino, N. Rowley, A.T. Kruppa, «A program for coupled-channel calculations with all order couplings for heavy-ion fusion reactions», *Comput. Phys. Commun.* **123**, 143 (1999).

[3] W. Greiner, R.K. Gupta, «Heavy Elements and Related New Phenomena», *World Scientific*, 1999.

[4] R. Lipperheide, H. Rossner, H. Massmann, «Calculation of reaction and fusion cross sections using angle-dependent phase shifts», *Nucl. Phys. A* **394**, 312 (1983).

[5] M. Beckerman, «Sub-barrier fusion of two nuclei», *Rep. Prog. Phys.* **51**, 1047 (1988).

[6] A.B. Balantekin, N. Takigawa, «Quantum tunneling in nuclear fusion», *Rev. Mod. Phys.* **70**, 77 (1998).

[7] M. Dasgupta *et al.*, «Measuring Barriers to Fusion», *Annu. Rev. Nucl. Part. Sci.* **48**, 401 (1998).

[8] H. Esbensen, «Fusion and zero-point motions», *Nucl. Phys. A* **352**, 147 (1981).

[9] M.A. Nagarajan, A.B. Balantekin, N. Takigawa, «Geometric interpretation of the adiabatic model for heavy-ion fusion», *Phys. Rev. C* **34**, 894 (1986). ónewpage

[10] K. Hagino, N. Takigawa, J.R. Bennett, D.M. Brink, «Effects of finite excitation energy of environment on fast quantum tunneling», *Phys. Rev. C* **51**, 3190 (1995).

[11] N. Rowley, G.R. Satchler, P.H. Stelson, «On the "distribution of barriers" interpretation of heavy-ion fusion», *Phys. Lett. B* **254**, 25 (1991).

[12] M. Dasgupta, D.J. Hinde, K. Hagino, «Barrier distributions as a tool to investigate fusion and fission», *Nucl. Phys. A* **630**, 78 (1998).

[13] J.R. Leigh *et al.*, «Barrier distributions from the fusion of oxygen ions with ^{144,148,154}Sm and ^{186}W», *Phys. Rev. C* **52**, 3151 (1995).

[14] `http://nrv.jinr.ru/nrv/`

[15] E.F. Aguilera, J.J. Kolata, R.J. Tighe, «Nuclear structure effects in the sub-barrier fusion of ^{16}O+^{70,72,73,74,76}Ge», *Phys. Rev. C* **52**, 3103 (1995).

[16] J. Fernández-Niello, C.H. Dasso, S. Landowne, «CCDEF — A simplified coupled-channel code for fusion cross sections including static nuclear deformations», *Comput. Phys. Commun.* **54**, 409 (1989).

[17] R.G. Stokstad *et al.*, «Fusion of ^{16}O+^{148,150,152,154}Sm at sub-barrier energies», *Phys. Rev. C* **21**, 2427 (1980).

[18] A. Morsad *et al.*, «Sub-barrier fusion of ^{28,30}Si with ^{24,26}Mg», *Phys. Rev. C* **41**, 988 (1990).

[19] A.M. Stefanini *et al.*, «Heavy-ion fusion below the Coulomb barrier: The systems ^{28,30}Si+^{58,62,64}Ni and ^{32,34,36}S+^{58,64}Ni», *Nucl. Phys. A* **456**, 509 (1986).

[20] S. Kalkal *et al.*, «Channel coupling effects on the fusion excitation functions for ^{28}Si+^{90,94}Zr in sub- and near-barrier regions», *Phys. Rev. C* **81**, 044610 (2010).

[21] D. Ackermann *et al.*, «Cross sections and average angular momenta in the fusion of ^{28}Si+^{94,100}Mo and ^{58,64}Ni+^{64}Ni», *Nucl. Phys. A* **609**, 1 (1996).

[22] H.Q. Zhang *et al.*, «Near-barrier fusion of ^{32}S+^{90,96}Zr: The effect of multi-neutron transfers in sub-barrier fusion reactions», *Phys. Rev. C* **82**, 054609 (2010).

[23] J. Khuyagbaatar *et al.*, «Evidence for hindrance in fusion between sulfur and lead nuclei», *Phys. Rev. C* **86**, 064602 (2012).

[24] H.G. Clerc *et al.*, «Fusion-fission and neutron-evaporation-residue cross-sections in ^{40}Ar- and ^{50}Ti-induced fusion reactions», *Nucl. Phys. A* **419**, 571 (1984).

[25] A.J. Najim, F.A. Majeed, K.H.H. Al-Attiyah, «Improved calculation of fusion barrier distribution», *IOP Conf. Ser. Mater. Sci. Eng.* **571**, 012124 (2019).

[26] L.F. Canto, R. Donangelo, «Improved determination of the fusion barrier distribution», *Phys. Rev. C* **79**, 037601 (2009).

[27] K. Hagino, «Investigating multichannel quantum tunneling in heavy-ion fusion reactions with Bayesian spectral deconvolution», *Phys. Rev. C* **93**, 061601(R) (2016).

[28] K.N. Sridhar, H.C. Manjunatha, H.B. Ramalingam, «Studies on the synthesis superheavy element $Z = 120$», *Nucl. Phys. A* **983**, 195 (2018).

[29] F.A. Majeed, R.S. Hamodi, F.M. Hussian, «Semiclassical coupled channels calculations in heavy-ion fusion reaction», *Adc. Stud. Theor. Phys.* **11**, 415 (2017).

[30] F.A. Majeed, Y.A. Abdul-Hussien, F.M. Hussian, «Fusion Reaction of Weakly Bound Nuclei in Nuclear Fusion», in: I. Girka (Ed.) «One Noble Goal and a Variety of Scientific and Technological Challenges», *IntechOpen*, London, UK 2019, pp. 186–186.

[31] G. Scamps, K. Hagino, «Coupled-channels description of multinucleon transfer and fusion reactions at energies near and far below the Coulomb barrier», *Phys. Rev. C* **92**, 054614 (2015).

[32] A.J. Toubiana, L.F. Canto, M.S. Hussein, «Approximate Transmission Coefficients in Heavy Ion Fusion», *Braz. J. Phys.* **47**, 31 (2017).

[33] V.I. Zagrebaev, V.V. Samarin, «Near-barrier fusion of heavy nuclei: Coupling of channels», *Phys. Atomic Nuclei* **67**, 1462 (2004).

[34] V.I. Zagrebaev, W. Greiner, «Synthesis of superheavy nuclei: A search for new production reactions», *Phys. Rev. C* **78**, 0346103 (2008).

[35] G. Montagnoli, A.M. Stefanini, «Recent experimental results in sub- and near-barrier heavy-ion fusion reactions», *Eur. Phys. J. A* **53**, 169 (2017).

[36] K. Siwek-Wilczyńska, J. Wilczyński, «Empirical nucleus–nucleus potential deduced from fusion excitation functions», *Phys. Rev. C* **69**, 024611 (2004).

[37] F.A. Majeed, F.M. Hussain, Y.A. Abdul-Hussien, «Enhanced calculations of fusion barrier distribution for heavy-ion fusion reactions using Wong formula», *Int. J. Nucl. Energy Sci. Technol.* **13**, 3 (2019).

[38] K. Hagino, N. Takigawa, «Subbarrier Fusion Reactions and Many-Particle Quantum Tunneling», *Prog. Theor. Phys.* **128**, 6 (2012).

[39] S.V.S. Sastry, S. Santra, «Structure information from fusion barriers», *Pramana* **54**, 813 (2000), `https://www.ias.ac.in/article/fulltext/pram/054/06/0813-0826`

[40] C.Y. Wong, «Interaction Barrier in Charged-Particle Nuclear Reactions», *Phys. Rev. Lett.* **31**, 12 (1973).

[41] D.L. Hill, J.A. Wheeler, «Nuclear Constitution and the Interpretation of Fission Phenomena», *Phys. Rev.* **89**, 5 (1953).

[42] R.H. Spear, «Reduced electric-octupole transition probabilities, $B(\mathrm{E3};0_1^+ \to 3_1^-)$, for even–even nuclides throughout the periodic table», *Atom. Data Nucl. Data Tables* **42**, 55 (1989).

[43] S. Raman, C.W. Nestor Jr., S. Kahane, K.H. Bhatt, «Predictions of $B(\mathrm{E2};0_1^+ \to 2_1^+)$ values for even–even nuclei», *Atom. Data Nucl. Data Tables* **42**, 1 (1989).